

Supplemental Information

3D printed materials with nanovoxelated elastic moduli

Peter L. H. Newman, Mohammad Mirkhalaf, Steven C. Gauci, Iman Roohani, Maté Biro, Christopher Barner-Kowollik, Hala Zreiqat

Detailed discussion on the constituents of the photoresist

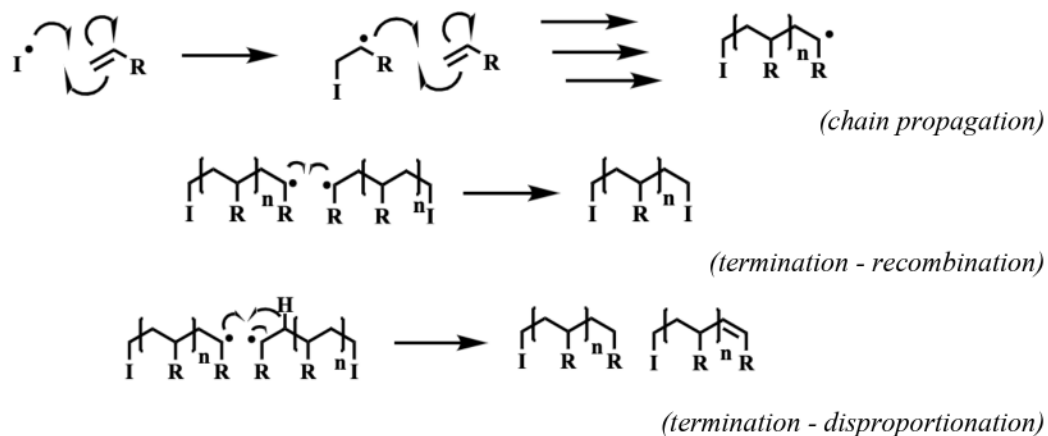
Our photoresist is designed to enable precise control over mechanical properties while ensuring rapid, high-resolution printing. Each component serves specific functions that work together to achieve these goals:

The Photoinitiator System: BAPO (phenylbis(2,4,6-trimethylbenzoyl)phosphine oxide) functions as a Type I photoinitiator, undergoing homolytic cleavage upon exposure to UV light to generate two reactive radical species:

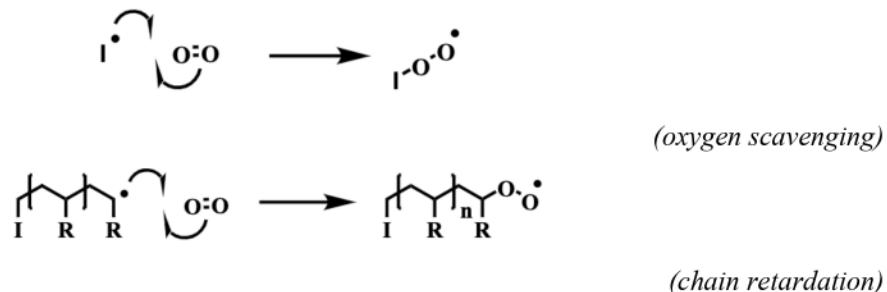


(photoinitiator excitation and cleavage)

These radicals typically initiate polymerization by reacting with prepolymers:



The Oxygen Management System: In standard photopolymerization, oxygen acts as a radical scavenger through two primary mechanisms:



To address this, our photoresist incorporates a glucose/glucose oxidase (G/GO) system that actively removes dissolved oxygen through enzymatic consumption:



This oxygen depletion enhances polymerization efficiency by (1) reducing scavenging of photoinitiator radicals, (2) decreasing termination of propagating polymer chains and (3) enabling complete cure at lower laser powers and exposure times.

Viscosity Control: Hydroxypropyl-methyl cellulose serves as a thickening agent, increasing the viscosity of the photoresist. This enhanced viscosity (1) restricts oxygen diffusion into the photoresist, (2) controls the spatial distribution of photoinitiated free radicals, (3) reducing radical termination through diffusion-based collisions.

Polymeric Components: The copolymer system comprises PEGDA250 and PEGDA575, which form the primary structural components of the printed material. The ratio between these components critically influences the (1) overall hydrophilicity/hydrophobicity balance, (2) network crosslinking density, (3) mechanical properties of the final printed structure (4) swelling behaviour in aqueous environments.

Solvent System: DMSO was selected as the solvent due to its (1) high solvating power for all components, (2) compatibility with the photoinitiator system, (3) ability to maintain stable solutions at high solute concentrations and (4) low volatility during printing.

Table S1. Overview of photoresist

Reagent	Concentration	Purpose / Mechanism
DMSO	Solvent	Ensures high solute compatibility in high concentrations
PEGDA250	10 wt%	Forms part of the copolymer hydrogel, structural component
PEGDA575	20 wt%	Forms part of the copolymer hydrogel, structural component
BAPO	Photoinitiator 65 g • L ⁻¹	Initiates polymerization upon exposure to light
Glucose	3.8 wt%	Part of the enzymatic oxidase system to limit oxidative inhibition of the polymerization reaction
Glucose Oxidase	0.23 wt%	Part of the enzymatic oxidase system to limit oxidative inhibition of the polymerization reaction
Hydroxypropyl-methyl Cellulose	2 wt%	Acts as a thickener to ensure high viscosity and limit oxygen transport, reducing oxygen inhibition of polymerization

Abbreviations: DMSO, dimethyl sulfoxide; PEGDA250, poly(ethylene glycol) diacrylate average Mn 250; PEGDA575, poly(ethylene glycol) diacrylate average Mn 575, BAPO, phenylbis(2,4,6-trimethylbenzoyl)phosphine oxide.

Swelling-induced internal stresses and early experiments exploring varied elastic modulus

Material failure in composite systems commonly occurs due to interfacial stresses generated between adjacent materials with mismatched mechanical properties. When such materials respond to external stimuli (temperature, moisture, mechanical load), the resulting strain differential creates internal stresses at material interfaces that can lead to catastrophic failure (*Gay, D. (2022) Composite Materials: Design and Applications. 4th edn. Boca Raton: CRC Press*). This fundamental mechanism manifests across diverse contexts in both everyday life and industrial applications. For example, in thermostats, the intentional thermal expansion mismatch between metals in bimetallic strips creates predictable bending, yet this same phenomenon can cause devastating delamination in electronic components where differential thermal expansion compromises structural integrity. In dentistry, differential swelling between synthetic composites and natural tooth structures generates interfacial stresses that can compromise dental restorations. Similarly, moisture-induced differential swelling in wooden structures, arising from variations in grain orientation or wood species, can result in severe structural failures through interface separation. Most relevant to our work, hydrogel-based biomedical devices like contact lenses frequently fail due to a delamination between layers of different compositions due to uneven swelling responses to hydration.

Our initial material development efforts encountered similar challenges. Early experiments exploring materials with varying elastic moduli - achieved through systematic variation of laser powers and voxel dwell times - revealed critical stability challenges. When these structures were exposed to water after fabrication, mismatched swelling ratios between adjacent regions led to catastrophic failure, with complete separation between different mechanical regions and detachment from the glass substrate (**Figure S1**). These observations directly motivated our development of a volume-conserving photoresist system that maintains consistent swelling behavior across regions of different elastic moduli, enabling the stable fabrication of elastically heterogeneous materials with nanoscale precision - the core advancement reported in our work.

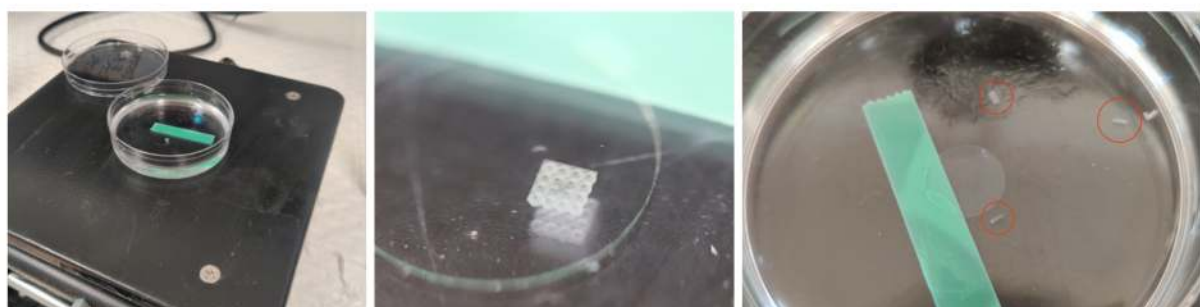


Figure S1. Material delamination due to differential swelling properties. Printed structures on a 10 mm coverslip maintained in DMSO solvent immediately after fabrication (left, middle panels) demonstrate initial structural integrity. Upon exposure to water (right panel), differential swelling between regions of different mechanical properties overcome material cohesion, resulting in delamination between material regions and complete detachment from the substrate (red circled regions show material floating).

Detailed discussion on copolymers for non-swelling

The swelling behavior of our photoresist emerges from the complex interplay between network architecture and molecular composition.

The polymerization of PEGDA monomers can be understood through graph theory, where individual PEGDA molecules represent nodes and crosslinks formed through acrylate polymerization represent edges. The number of connections to a given PEGDA molecule (node degree) determines the local network architecture and consequently influences both mechanical and swelling properties. Three primary network architectures can form during polymerization. Linear chains occur when each PEGDA connects to exactly two others (degree 2), forming flexible chains with minimal crosslinking. These structures maintain significant chain mobility and retain a high proportion of unreacted acrylate groups. Branched networks form when PEGDA molecules create Y-shaped junction points (degree 3), resulting in partially crosslinked networks with moderate numbers of unreacted acrylates. Finally, fully crosslinked networks (degree 4) represent maximum connectivity, forming dense networks with minimal unreacted acrylates and restricted chain mobility.

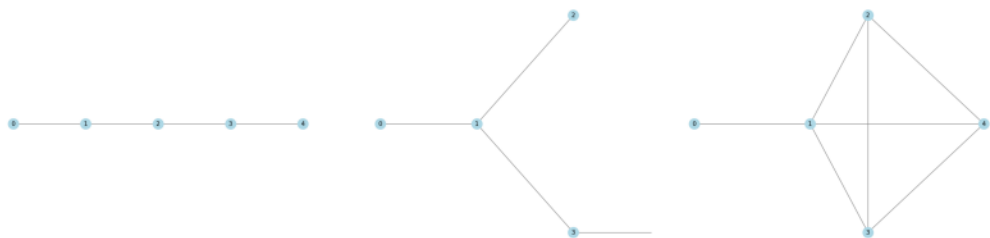


Figure S2: Graph representation of polymer network architectures. Linear chains showing degree 2 connectivity (left). Branched networks with degree 3 nodes (middle). Fully crosslinked networks achieving degree 4 connectivity (right). Nodes represent PEGDA molecules, edges represent crosslinks, and red dots indicate unreacted acrylate groups.

The overall swelling behavior results from competing molecular interactions. The PEG backbone provides hydrophilicity, with longer chains (PEGDA575) contributing more than shorter ones (PEGDA250). Conversely, acrylate end groups and crosslink points introduce hydrophobic character and restrict water uptake. Different network architectures, with their varying degrees of unreacted acrylates, therefore, exhibit different hydroscopic behaviors.

The Flory-Rehner equation provides a theoretical framework for understanding swelling in a polymer.

$$\ln(1-v') + v' + \chi v'^2 = (\rho V/M_c)(v'^{(1/3)} - v'/2)$$

where v' represents polymer volume fraction in the swollen state, χ is the polymer-solvent interaction parameter, ρ is polymer density, M_c is molecular weight between crosslinks, and V_1 is solvent molar volume. Higher crosslink density (lower M_c) and more hydrophobic regions (higher χ) both reduce swelling, while network architecture influences both parameters simultaneously.

Achieving volume conservation (swelling ratio ≈ 1) requires carefully balancing network architecture, end-group hydrophobicity, and polymer network properties, through optimization of the PEGDA250:PEGDA575 ratio, laser exposure parameters, and total polymer concentration. Our exploration of this parameter space revealed conditions where regions of dramatically different mechanical properties maintain consistent volume conservation, enabling the fabrication of mechanically heterogeneous structures without delamination or distortion.

OpenScribe: Software for Nanoscale Mechanical Property Control

OpenScribe is a Python-based software platform designed to enable the fabrication of materials with programmable elastic properties at the nanoscale. The software bridges the gap between design intent and practical fabrication through several key innovations in multiphoton lithography control. Compatible with Nanoscribe's GWL file standard, OpenScribe introduces direct specification of mechanical properties within printed structures, automatically translating desired elastic modulus values into optimized laser parameters.

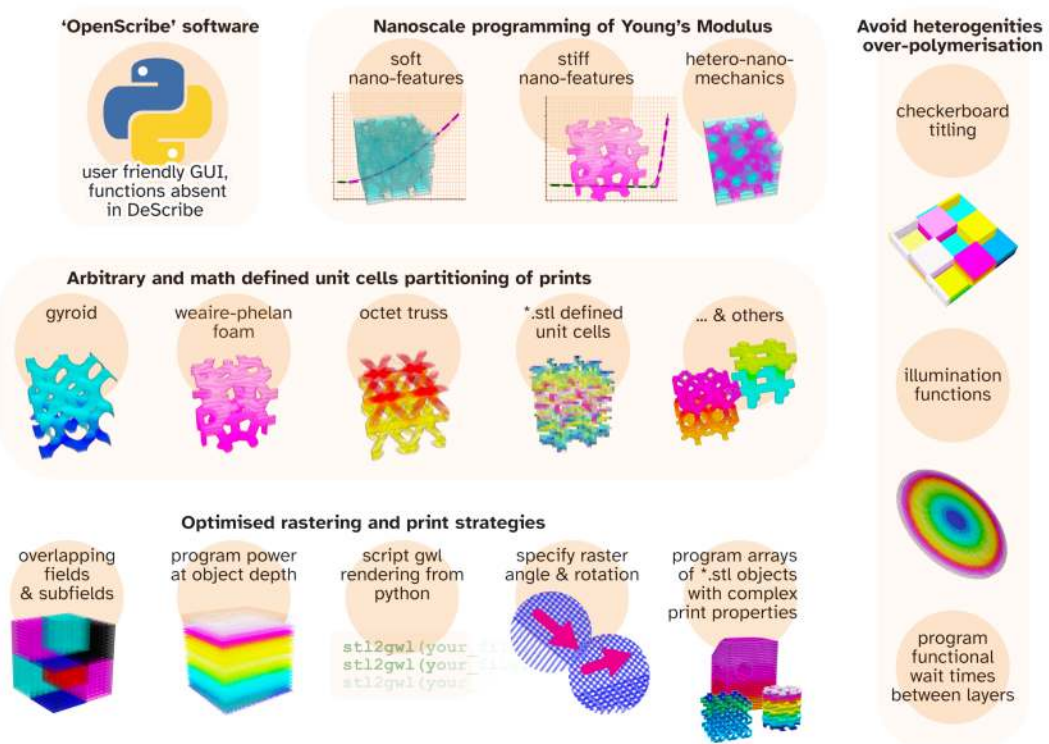


Figure S3. OpenScribe – a software for programming nanoscale regions of well-defined elasticity.

The software's core capabilities include:

- Direct mechanical property programming through an intuitive interface
- Complex periodic structure generation with built-in unit cell templates
- Advanced process control for consistent fabrication conditions
- Multi-object printing with precise spatial and temporal coordination
- Field and subfield printing strategies for optimized polymerization

The OpenScribe graphical user interface enables precise control over material properties and printing parameters through a notebook-based workflow:

- Object definition: STL files are loaded and organized within a print notebook
- Property assignment: Mechanical properties are specified through direct elastic modulus input
- Process optimization: Print parameters including laser power, hatching patterns, and illumination fields are automatically configured
- Multi-object coordination: Multiple objects can be defined and printed with independent properties
- Quality control: visualization tools enable preview and verification of print parameters

The software is available as an open-source project, encouraging collaborative development and customization across disciplines. The following table provides a detailed comparison between OpenScribe's capabilities and traditional multiphoton printing software (DeScribe), highlighting the novel features that enable precise control over mechanical properties at the nanoscale

Below in **Figure S4** is a screen shot of the OpenScribe app that was created for the current software. Printed objects are loaded in the STL format and can then be manipulated with a variety of different slicing and power transformations. Each object the user desires to be printed created a new print page within the printing notebook. Use input define the properties of the given object within the print page of that complete notebook. As many objects as the user desired can be added to the one print notebook. The code is all available open source. The below table outlines all of the functions that are include within the software. This is compared to NanoScribe's DeScribe software.

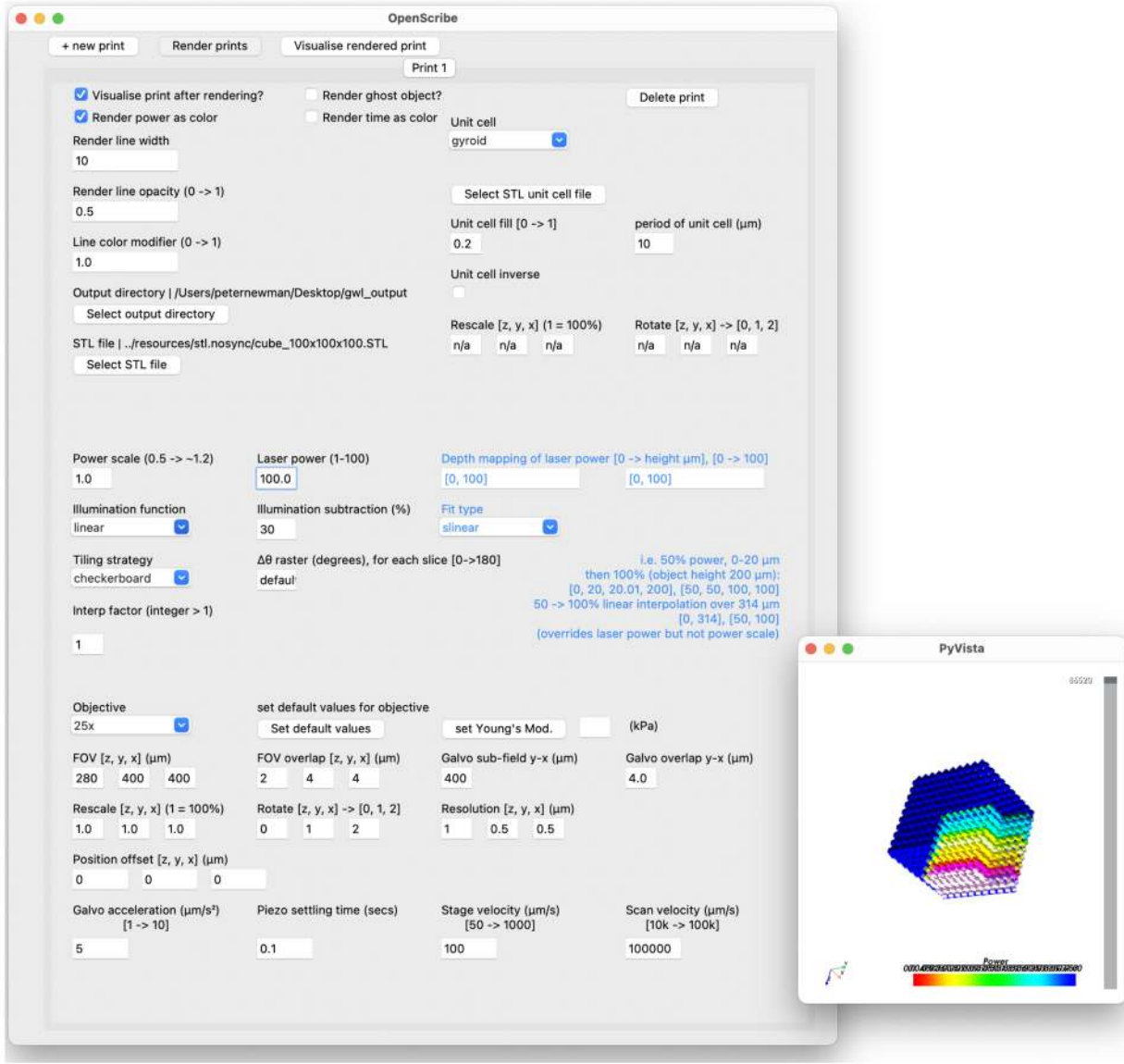


Figure S4. The OpenScribe software. A typical view of OpenScribe software having rendered a cube object for printing with a gyroid unit cell structure.

Table S2. Overview of novel features of the OpenScribe software in comparison with DeScribe

Feature 1. Direct programming of object elastic modulus

OpenScribe is the first software tool designed specifically for creating materials with programmable elastic properties at the nanoscale. This software bridges the gap between conceptual design and practical fabrication through several key innovations

Direct Mechanical Property Control:

- Specification of target elastic modulus values within 3D geometries
 - Automated translation of mechanical properties to laser parameters
 - Integration of experimental photoresist characterization data

Metamaterial Design Tools:

- Efficient handling of periodic unit cell structures
 - Built-in mathematical structure templates (gyroid, octet truss, etc.)
 - Optimized mesh processing for complex geometries
 - Custom unit cell import via STL files

Process Control Functions:

- Field illumination compensation algorithms
 - Layer-by-layer parameter adjustment
 - Local heating and radical diffusion management
 - Print sequence optimization

Hardware Interface Capabilities:

- Multi-object printing coordination
 - Height-dependent laser power compensation
 - Variable hatching angle control
 - Field/subfield printing strategies

The software provides both a scriptable environment and graphical user interface, with cross-platform compatibility (Windows, macOS, Linux) to facilitate collaborative development. The following table details specific features and their implementation.

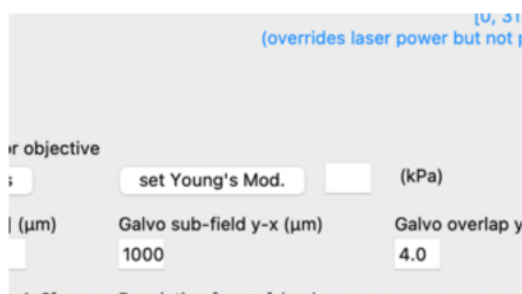
The '*set elastic modulus*' button and field allows users to specify target mechanical properties. To use:

1. Enter the desired elastic modulus value in the field to the right of the button
 2. Press the button to apply settings
 3. The software will automatically adjust resolution, laser hatching values, and laser power

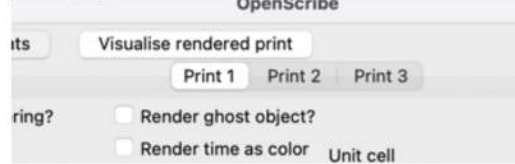
During processing, the software:

- Creates a digital 3D array representing the voxelated object from the STL file
 - Maps desired mechanical properties to optimized laser parameters using experimentally-validated relationships
 - Generates machine instructions including scanning paths and power modulation commands
 - Applies process corrections for field illumination and height-dependent effects

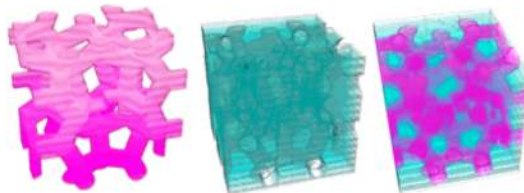
Note: Parameter mapping is calibrated for the volume-conserving photoresist detailed in this work.



The addition of multiple ‘objects pages’ with the ‘print notebook’ i.e.: ‘Print 1 / 2 / 3’ pages.



Permits nested mechanically voxelated structures, i.e.:



Feature 2. OpenScribe is an open-source python project

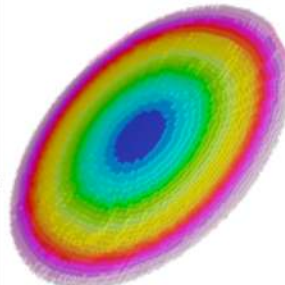
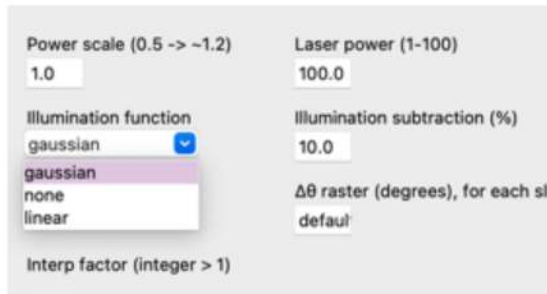
- OpenScribe is available at the Authors github page to be forked and altered by anyone
- Written in Python for simplicity and widespread adoption
- Can run on any computer with python – Windows, MacOS, Linux

By comparison, DeScribe is a proprietary and close licensed software that is limited to Windows

Feature 3. Illumination functions across a x-y slice

OpenScribe allows users to define spatial variations in illumination intensity across the print field:

1. Access the illumination control panel via the 'Set Illumination' dropdown box



2. Choose from predefined functions or input custom intensity distributions
3. Preview the resulting illumination pattern in the visualization window

This strategy is implemented as a global print parameters rather than dynamically calculated object-specific optimisations.

Local variations in photopolymerization can arise from:

- Heat accumulation in densely printed regions
- Concentration gradients of photochemical species
- Oxygen diffusion patterns
- Light scattering effects at the material interfaces

Illumination compensation helps address:

- Spatial heterogeneity in crosslinking density
- Variations in mechanical properties
- Inconsistent feature resolution

-
- Print failures due to local overexposure

The software implements:

- Intensity modulation
- Position-dependent laser power adjustment
- Layer-by-layer illumination control
- Field subdivision for precise exposure management

The Gaussian-based compensation is implemented within the OpenScribe software through the following steps:

1. Calculate sigma based on the use of a unit cell or the field of view:

```
if print_prop.unit_cell_fill < 1:
    sigma = (print_prop.unit_cell_period / 2) * print_prop.unit_cell_fill
    sigma = np.argmin(np.abs(x[0, :] - x[0, :].min() - sigma))
else:
    sigma = len(x) // 2
```

2. Calculate padding based on the Gaussian sigma parameter (The padding amount is set to either 3 times sigma or half the image size, whichever is smaller. A binary mask identifies the print regions):

```
pad_amount = min(int(np.round(3 * sigma)), x.shape[0] // 2)
mask = v == 1
```

3. Prepare and pad the volume for filtering (the volume is padded with zeros and inverted to prepare for filtering):

```
v_blur = np.pad(v, pad_amount, mode="constant")
v_blur = np.abs(v_blur.astype("float32") - 1)
```

4. Apply filtering and crop (a Gaussian filter smooths the boundaries, then the padding is removed):

```
v_blur = gaussian_filter(v_blur, sigma=sigma)
v_blur = v_blur[pad_amount:-pad_amount, pad_amount:-pad_amount]
```

5. Normalize and scale (normalized to [0,1] and scaled by the user-defined power adjustment)

```
v_blur -= v_blur.min()
v_blur *= mask
v_blur /= np.max(v_blur)
v_blur *= print_prop.illumination_function_minus
```

6. Apply final power adjustments (base laser power is added and non-print regions are set to constant power):

```
v_blur += print_prop.laser_power
v_blur -= print_prop.illumination_function_minus
v_blur[~mask] = print_prop.laser_power
```

The linear distance-based illumination compensation follows a similar pattern:

1. Initialize and pad the power map

```
p = np.pad(ones, 1, mode="constant")
```

2. Calculate distance transform (pixel distance from edge of object, Euclidean distance from feature boundaries is computed):

```
p = cv2.distanceTransform(p.astype("uint8"), cv2.DIST_L2, 3)
```

3. Power is scaled linearly with distance and clipped to valid range:

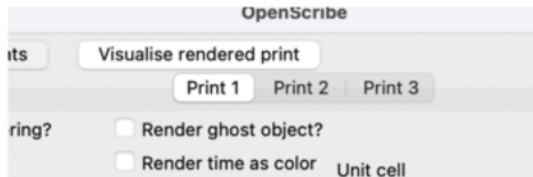
```
p = print_prop.laser_power * (1 - (print_prop.illumination_function_minus /
100) * (p / np.max(p)))
p = np.clip(p, 0, print_prop.laser_power)
```

These implementations generate power maps that modulate laser intensity based on local geometry, helping maintain consistent polymerization conditions throughout the print volume. Therefore, both illumination correction functions result in a printed slice with a maximum power specified by “Laser power (1-100)” within the OpenScribe software, and a minimum laser power specified by “illumination subtraction %” within the OpenScribe software. The value between this maxima and minima are geometry dependent.

Feature 4. Multi-object printing

OpenScribe enables simultaneous definition and control of multiple print objects:

-
1. Create new object entries using the '+ new print' button in the print notebook
 2. Each object gets its own configuration page for independent parameter control
 3. Objects can be positioned with arbitrary spacing in 3D space
 4. Preview all objects in the visualization window to verify placement



Print sequence optimization:

- Automatic Z-height sorting
- Layer-by-layer processing across objects
- Intelligent path planning to minimize travel time
- Collision avoidance for close-packed structures

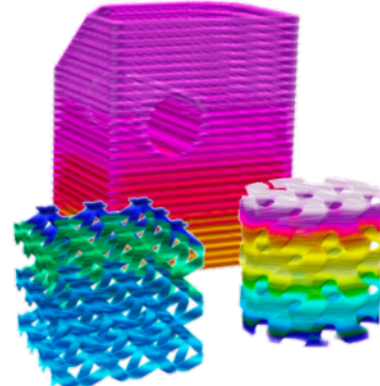
Parameter control:

- Independent mechanical properties per object
- Object-specific illumination settings

Advanced applications:

- High-throughput parameter sweeps
- Combinatorial material studies
- Nested mechanical structures
- Interpenetrating object geometries

The software generates a master print file ('*_job.gwl') that coordinates all objects' fabrication sequences while maintaining precise spatial and temporal control. This enables printing objects in close proximity or even nested within each other - capabilities not typically available in standard multiphoton printing software.



By comparison, this function is possible using DeScribe, though DeScribe limits the proximity of objects. In DeScribe objects are printed one at a time, such that they must be placed far apart, and the objective will not crash into subsequent prints. This is also the same for multiparameter sweeps, which limits the total number of parameters that can be efficiently spaced on a given substrate. Material properties can not be specified.

Feature 5. Simple programming of laser power at arbitrary 'z-depth'

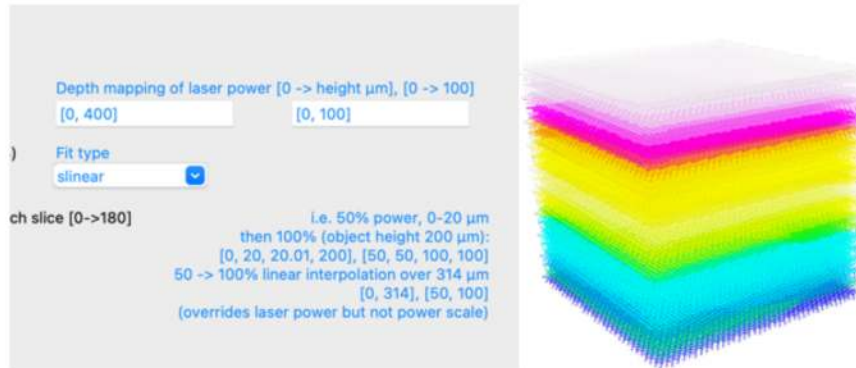
Simple programming of laser power at arbitrary 'z-depth'. The software adjusts laser power based on the specified depth function to maintain consistent polymerization conditions throughout the print volume. This compensation is particularly critical in oil immersion mode, where power transmission decreases exponentially with depth due to optical effects and material interactions.

The software supports power compensation using a depth-mapping function $P(z) = P_0 * f(z)$, where P_0 is the initial power and $f(z)$ is a piecewise linear interpolation. We note that practical implementation requires careful characterisation of depth-dependent transmission effects and compensation for optical phenomena like reflection and refraction through the printed structure – these compensations are not made by the OpenScribe software.

This strategy is implemented as a global print parameters rather than dynamically calculated object-specific optimisations.

User interface controls:

1. Enter depth-power pairs as a list in the depth mapping and height fields
2. Select interpolation method from the dropdown menu
3. Preview the resulting power curve in the visualization window (via ‘render print’ with the ‘view laser power as color’ checkbox enabled)
4. Apply settings across selected objects or layers



Power compensation methods:

- Linear interpolation between defined points
- Polynomial fitting for smooth transitions
- Custom depth function definition

Depth-dependent effects addressed:

- Optical path length variations
- Material absorption and scattering
- Refractive index mismatches
- Focus degradation with depth

Applications:

- Oil immersion printing optimization
- Deep structure fabrication
- Multi-layer composite materials
- Consistent feature size across depths

Feature 6. Program hatching angle, and change between slices

OpenScribe allows a user to specify changes in the raster angle between slices of a print:

User interface controls:

1. Access hatching controls via the 'Δtheta raster (degrees)' field
2. Define angle variation patterns between layers
3. Preview resulting scan patterns in the visualization window



Changing the raster angle can help prevent heterogeneities in a print that develop due to object geometry. Such ‘hot spots’ of heat and photochemical radicals, as well as inhibitory species such as oxygen. Complex and non-linear interactions between such hot spots can lead to uneven printing.

This strategy is implemented as a global print parameters rather than dynamically calculated object-specific optimisations.

Process considerations addressed:

- Local heat accumulation
- Radical concentration gradients
- Oxygen diffusion patterns

Applications:

- Homogeneous crosslinking density
- Reduced thermal accumulation
- Enhanced mechanical isotropy

Advanced applications:

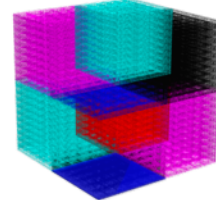
- Multi-pass scanning strategies
- Region-specific hatching patterns

Feature 7. Program field and subfields within a print

Enter field parameters in designated input fields:

1. 'FOV': Sets the total field of view
2. 'FOV overlap': Defines overlap between adjacent fields
3. 'Galvo-sub-field y-x': Specifies subfield dimensions
4. 'Galvo overlap': Sets overlap between subfields

FOV [z, y, x] (μm) 280 400 400	FOV overlap [z, y, x] (μm) 2 4 4	Galvo sub-field y-x (μm) 400	Galvo overlap y-x (μm) 4.0
---	---	---------------------------------	-------------------------------



This strategy is implemented as a global print parameters rather than dynamically calculated object-specific optimisations.

Technical implementation - subfields are sequentially rastered subvolumes where:

- Stage remains stationary
- Only galvo movement is used
- Each subfield is completely processed before moving to the next
- Overlaps ensure seamless transitions

Process benefits:

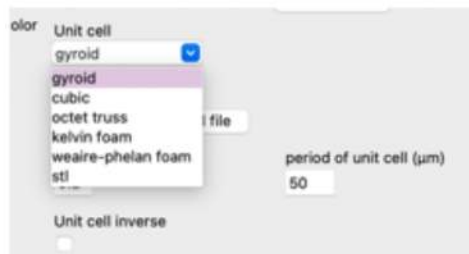
- Reduces heat accumulation in any single region
- Allows dissipation of photochemical reaction products
- Minimizes oxygen diffusion effects
- Promotes more uniform polymerization conditions

This approach helps prevent print heterogeneities by breaking large volumes into smaller, manageable sections that can be processed under more consistent conditions.

Feature 8. Specify complex internal unit cell rendering of a print object

User interface controls:

1. Select unit cell type from dropdown menu
2. Specify unit cell period (defines scaling)
3. Toggle 'unit cell inverse' checkbox to:



Standard mode: Creates specified unit cell structure

Inverse mode: Creates complementary void space unit cell structure

Available unit cell types:

- Gyroid
- Cubic
- Octet truss
- Kelvin foam
- Weaire-Phelan
- Custom unit cells for a user specified *.stl file



Technical implementation:

- Mathematical generation of periodic structures
- Automatic scaling based on period parameter
- Direct rendering within OpenScribe
- Integration with other print parameters

This feature enables rapid generation of complex periodic structures commonly used in metamaterial design without requiring external CAD software.

By comparison, this can be compete outside of DeScribe with CAD tools including nTopology etc, the intricacies introduced within such object files can make such files (~ GBs) unmanageable by DeScribe.

The biological functionality of our photoresist can be precisely controlled through the concentration of conjugated biomolecules. Using laminin as a model protein, we demonstrated concentration-dependent cell attachment. The base photoresist without laminin shows minimal cell attachment, confirming its bio-inert properties. Increasing laminin concentrations (0, 12, 25, and 50 $\mu\text{g}/\text{mL}$) led to proportionally increased cell attachment, demonstrating specific control over biological functionality through biomolecule conjugation.

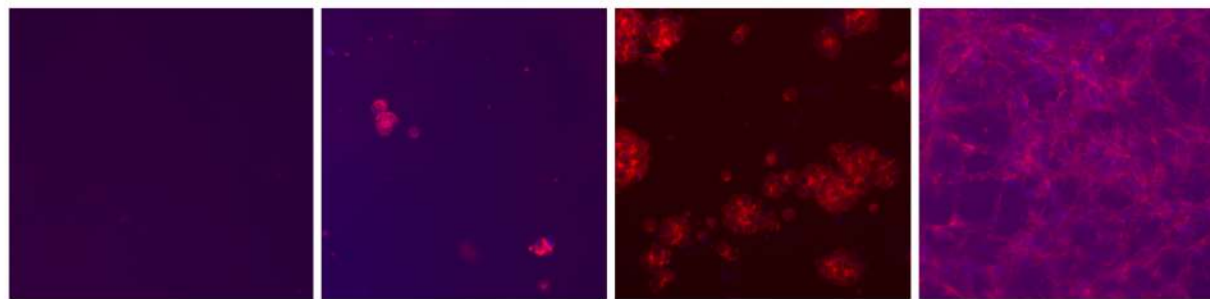


Figure S5. Concentration-dependent cell attachment to laminin-functionalized photoresist. Epi-fluorescent imaging of human pluripotent stem cells attachment to photoresist surfaces functionalized with different concentrations of laminin (left-to-right 0, 12, 25, and 50 $\mu\text{g}/\text{mL}$). Blue shows cell nucleus and red cell actin. The control (0 $\mu\text{g}/\text{mL}$) shows minimal cell attachment, demonstrating the intrinsically bio-inert nature of the base photoresist. Increasing laminin concentration correlates with increased cell attachment, confirming specific biological functionality through controlled biomolecule conjugation.

To promote the highest possible writing speeds, the saturation limit of BAPO in DMSO was experimentally measured using UV-Vis absorption, establishing BAPO could be used at 65 mg $\cdot \text{mL}^{-1}$.

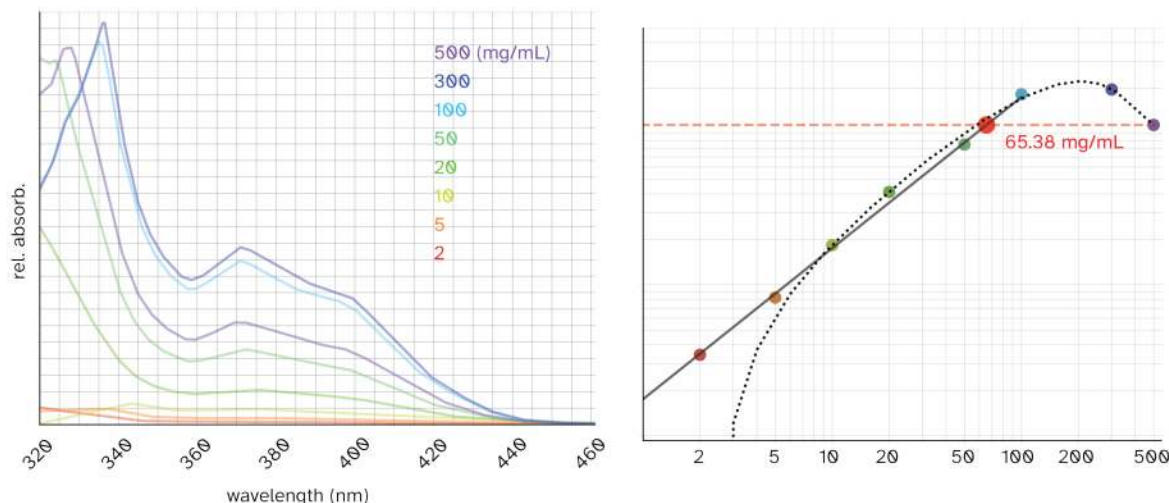


Figure S6. Saturation of photoinitiator BAPO in DMSO

Representative examples of the raw force spectroscopic data, with fits, as per calculations https://github.com/peterlionelnewman/force_spectroscopy. Elastic moduli were calculated using a neo-hookean Ogden Hertz-fit model from force curves using the code – as detailed in the available code repository.

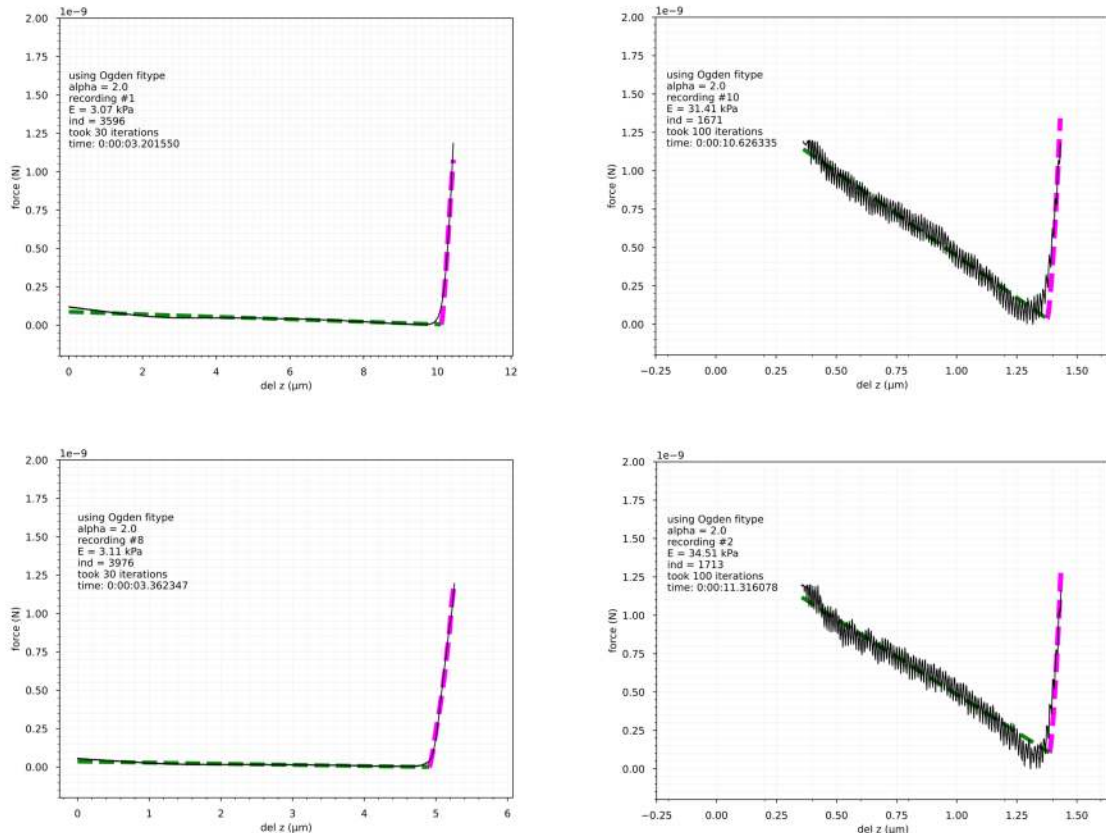


Figure S7. Raw force-displacement curves

An alternative presentation of the 3D plotted data presented in Figure 2. The plots are presented in a 2D format showing the relationship between hatch volume, laser power, and elastic modulus. Splines-of-best-fit are plotted to highlight trends. Violin plots are overlaid with a box plot showing the mean and 1st/3rd quartile values. Power is presented as a percentage of the 50 mW calibration value of the NanoScribe GT2.

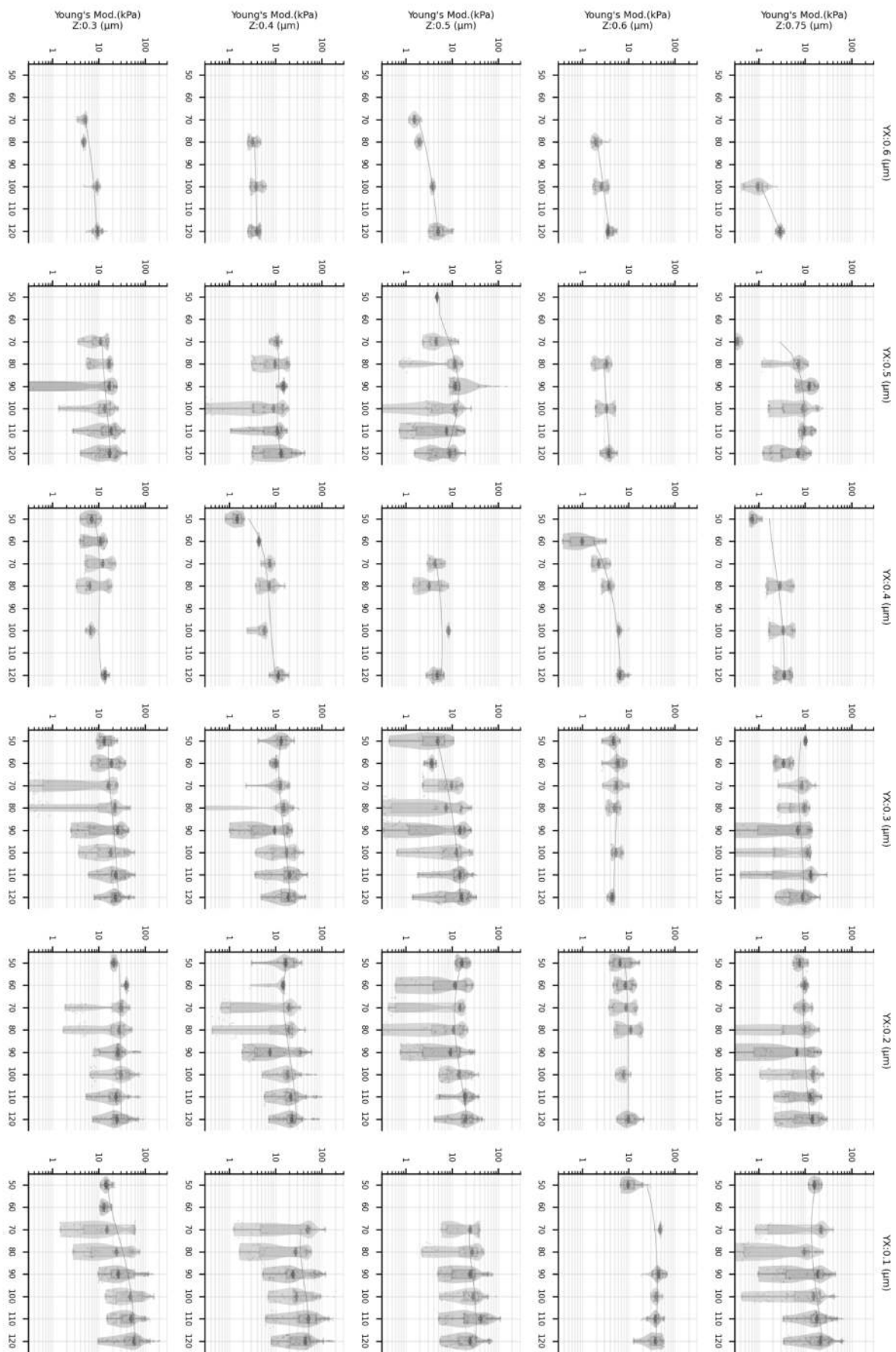


Figure S8. The complete set of the hatch volume, elastic modulus data at different laser powers, shown in Figure 2b in the 3D data set, shown here in arrays of 2D data.

Representation of the 3D plotted data presented in Figure 2 shown with the interpolation line / surface over which elastic moduli are calculated.

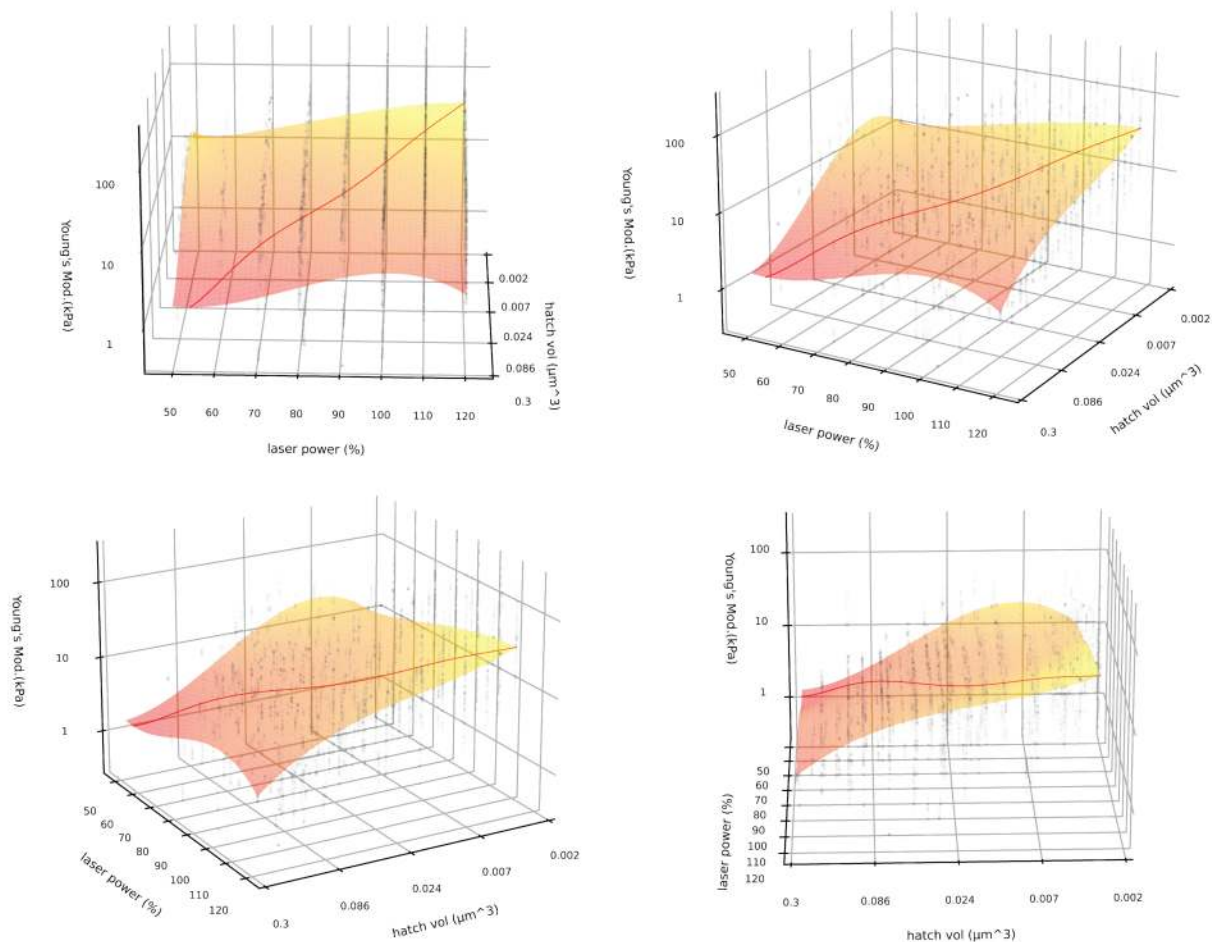


Figure S9. The line over which elastic moduli is interpolated (used within the OpenScribe software) given a laser power and hatch volume.

A slice of the raw confocal imaging data used to generate 3D renders of the printed structures, (prior to tile illumination correction, alignment and blending).

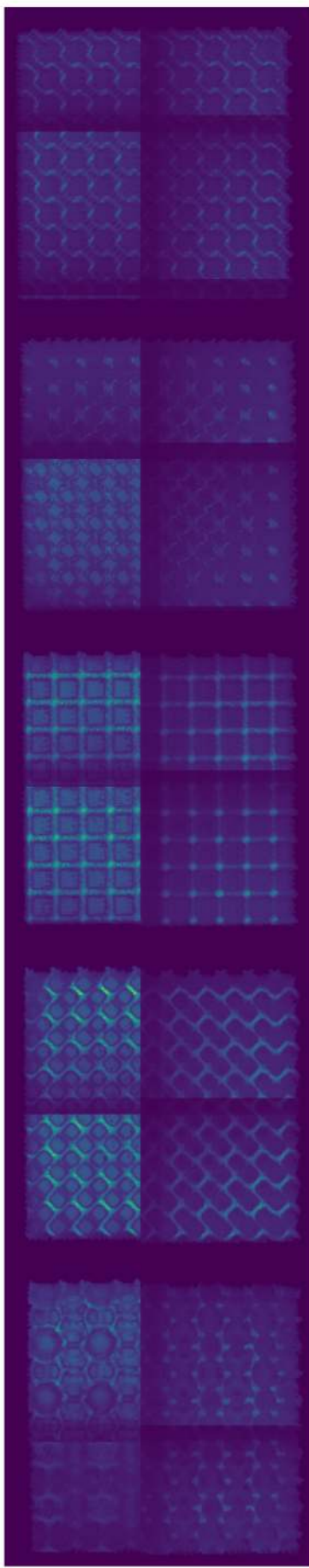


Figure S10. Raw confocal microscopy data of printed unit cell structures. Images were acquired using a Zeiss LSM 800 Confocal microscope with $63\times$ objective (NA 1.40), exploiting the natural UV autofluorescence of PEG. Brighter regions indicate higher local polymer density, providing intrinsic contrast that reveals mechanically heterogeneous regions without additional labels. Raw data shown prior to tile illumination correction, alignment and blending. Imaging parameters: excitation wavelength = 405 nm, emission collected >420 nm, pinhole = 1.0 AU, pixel size ~ 0.4 μm . Additional imaging details can be found in Methods.

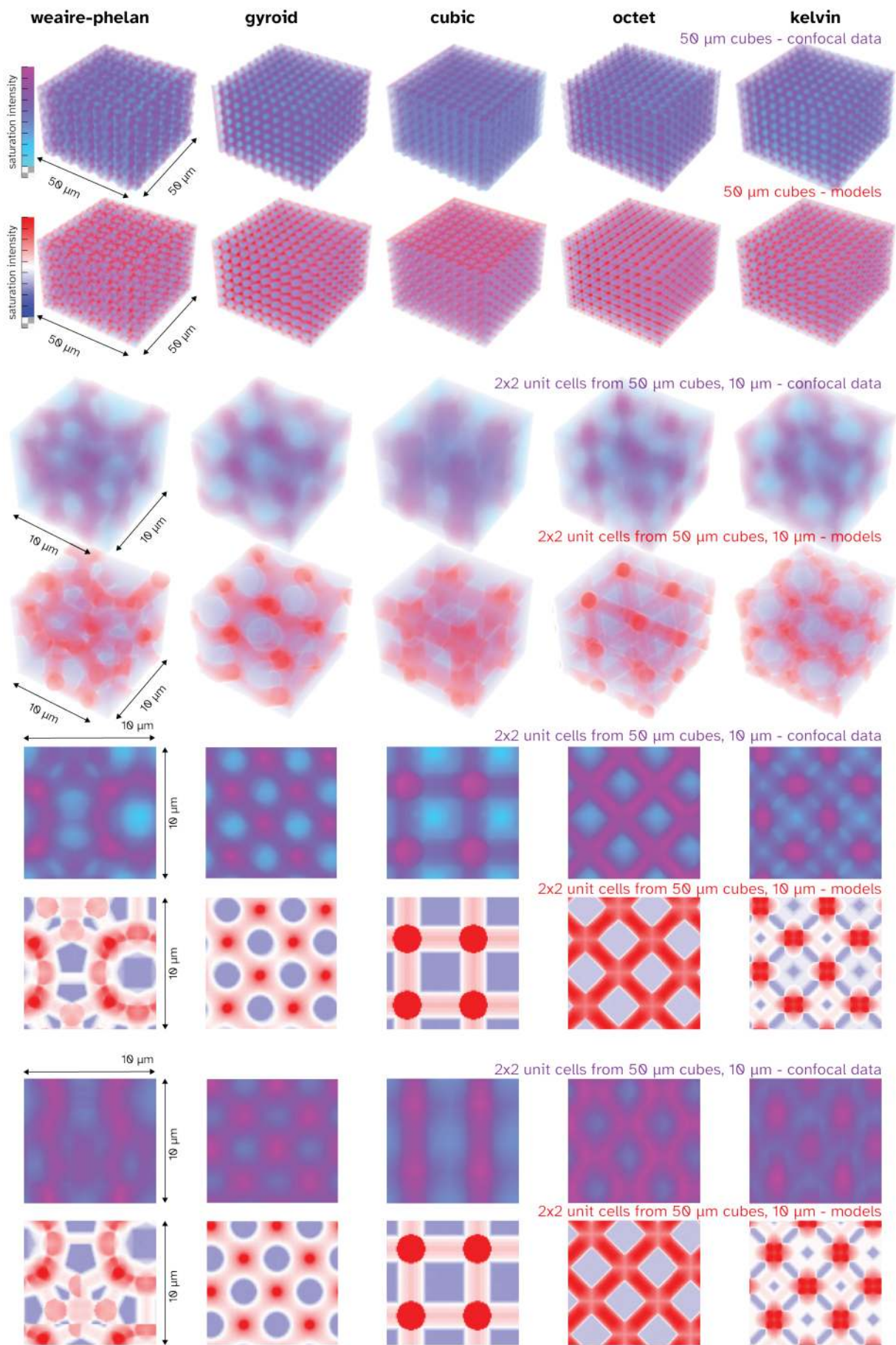


Figure S11. A summary of the confocal data taken of 5 different materials with complex voxelated mechanics. Cyan and magenta confocal data is shown alongside theoretical renders of the same structure rendered in blue and red. 5 columns are shown of 5 different unit cells. Row 1 and 2 shows the entire 50 μm cube, with 10 unit cells in x y direction and 7 in the z direction. Row 3 and 4 shows a 2x2 sized unit cell of the data in the top row that enlarged. Row 5-8 show xy mean slices of confocal and theoretical data, as well as xz mean slice of the confocal theoretical data.

Extended Discussion on the Measurement of Elastic Maps

In our study, force maps exhibiting heteromechanical properties were conducted in quadruplicate, sampling 6,400 locations over a 10 $\mu\text{m} \times 10\mu\text{m}$ area. This corresponds to a spatial resolution of 125 nm per pixel (80 pixels per line). Scanning with a higher spatial resolution offers several advantages. High-resolution scanning enables the mapping of steep mechanical gradients and the identification of subtle variations in mechanical properties that might be missed with a coarser grid. This includes the use of a model-based super-resolution approach, with parametric functions to infer limits beyond the Nyquist-sampled data. Additionally, a higher pixel density enhances statistical reliability by reducing the impact of noise and local anomalies. Further, in the stiffer regions, where the contact radius is smaller, the high spatial resolution approaches the Nyquist sampling limit, allowing for more accurate measurements (see calculations below). We employed a 10 μm diameter polystyrene (PS) bead as the indenter in an AFM setup submerged in an aqueous environment to maintain the integrity of the hydrogel samples. The choice of a 10 μm colloidal probe involved several critical considerations. Although a larger probe increases the contact area, it provides a more reliable average of the bulk mechanical properties, reducing the influence of the hydrogel's microstructure. Smaller, sharper tips (e.g., conical or pyramidal) offer higher nominal spatial resolution but risk penetrating soft hydrogels with elasticity in the kilopascal (kPa) range [doi.org/10.1038/s41596-021-00495-4], leading to inaccurate measurements and potential sample damage. Further, in our testing, radii smaller than 5 μm caused significant electrostatic interactions with soft materials, making the probes too 'sticky' thereby compromising measurement reliability. Such reliability was essential since hydrogel materials necessitate an aqueous environmental chamber with consistent submersion – introducing further noise and drift.

To assess the spatial resolution limits imposed by our experimental setup, we performed calculations based on Hertzian contact mechanics. The contact radius between a spherical indenter and an elastic half-space is given by:

$$\text{Contact Area} = \frac{3}{4} \left(\frac{(Force \sim 1 \text{ nN}) \cdot (radius \sim 5 \mu\text{m})}{Elastic Mod.} \right)^{1/3} \overline{1 - (poisson ratio \sim 0.5)^2}$$

For *Elastic Mod.* $\approx 3 \text{ kPa}$ | 30 kPa : Contact Area $\approx 965 \text{ nm}$ | 448 nm

The finite size of the contact area suggests that the spatial resolution of our mechanical measurements may be limited by the contact radius rather than the pixel size (125 nm). The observed mechanical transition width of 770 nm is within the range defined by the contact radii. This suggests that the transition width may represent an upper bound constrained by the probe's contact area. Consequently, the actual mechanical transition in the material could be sharper than our measurements indicate. The calculations based on Hertzian contact mechanics support our observations and provide confidence in the robustness and reliability of our method. Acknowledging the limitations imposed by the contact area enhances the validity of our findings and underscores the precision achieved in fabricating materials with nanovoxeleted elastic moduli.

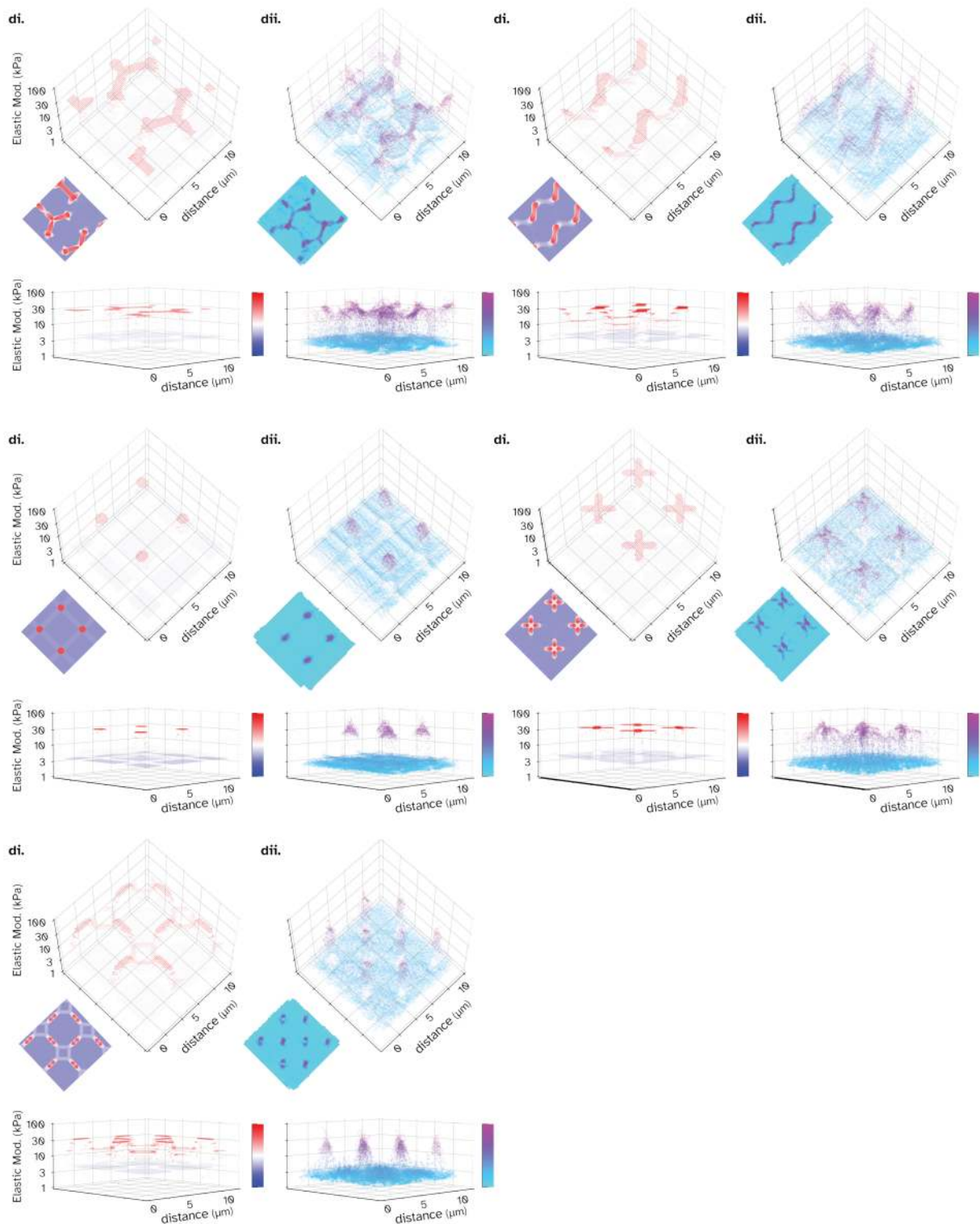


Figure S12. Elastic maps of all the soft-stiff tessellated units cells fabricated and measured for this work with complex nano voxelated mechanics.

Color-coded plots of the elastic maps for the soft-stiff printed structures are shown below. Replicate data (4 replicates) is presented in a 2-by-2 grid as rotated/aligned prior to calculating the mean elasticity used in the calculation of the soft-stiff transition region (see Methods).

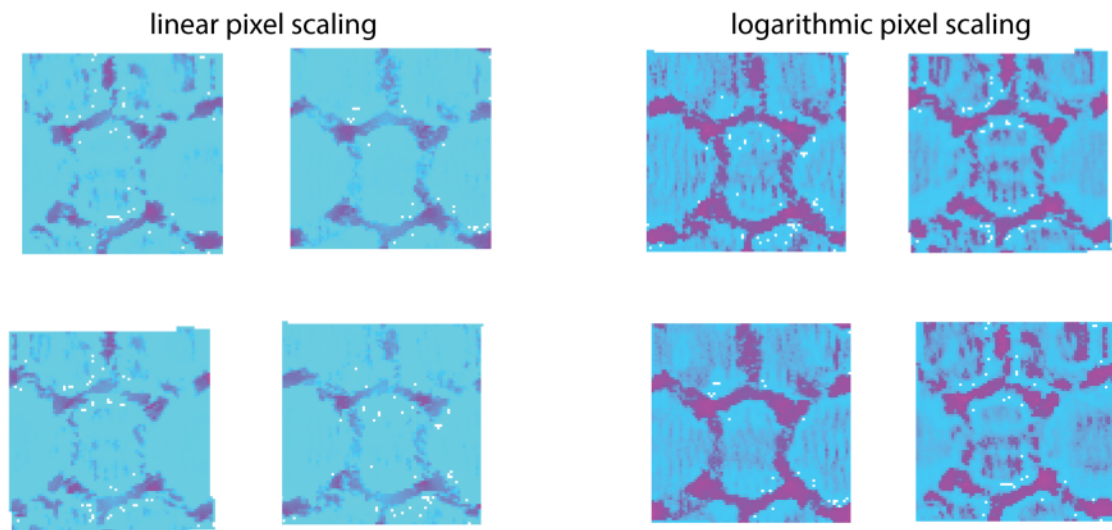


Figure S13. The elastic maps of the Weaire-Phelan unit cell array.

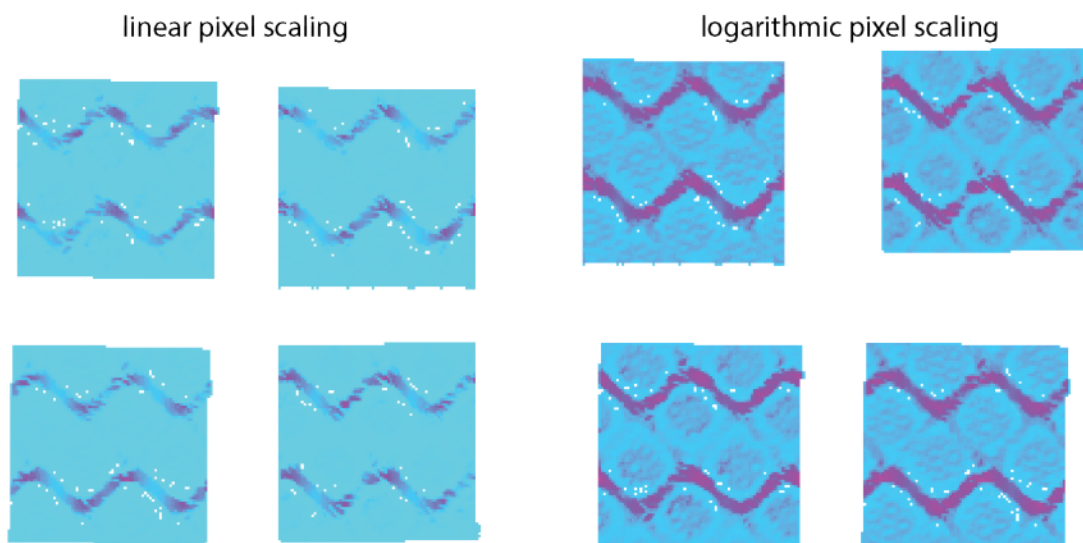


Figure S14. The elastic maps of the gyroid unit cell array.

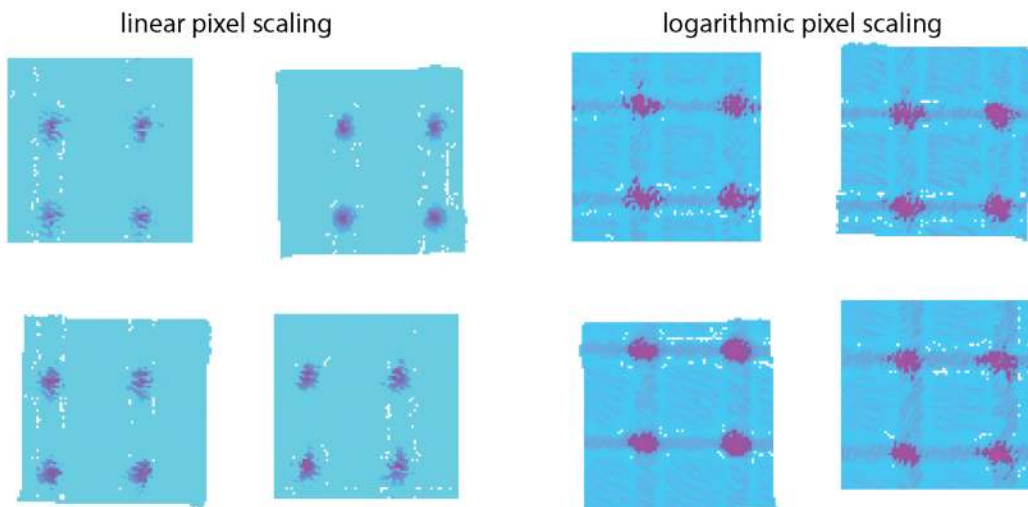


Figure S15. The elastic maps of the cubic unit cell array.

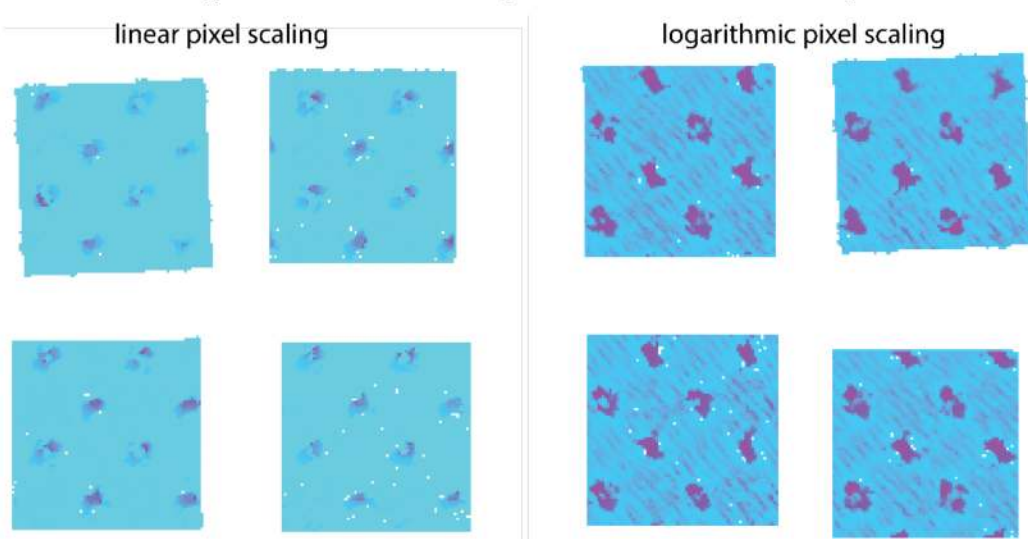


Figure S16. The elastic maps of the octet truss unit cell array.

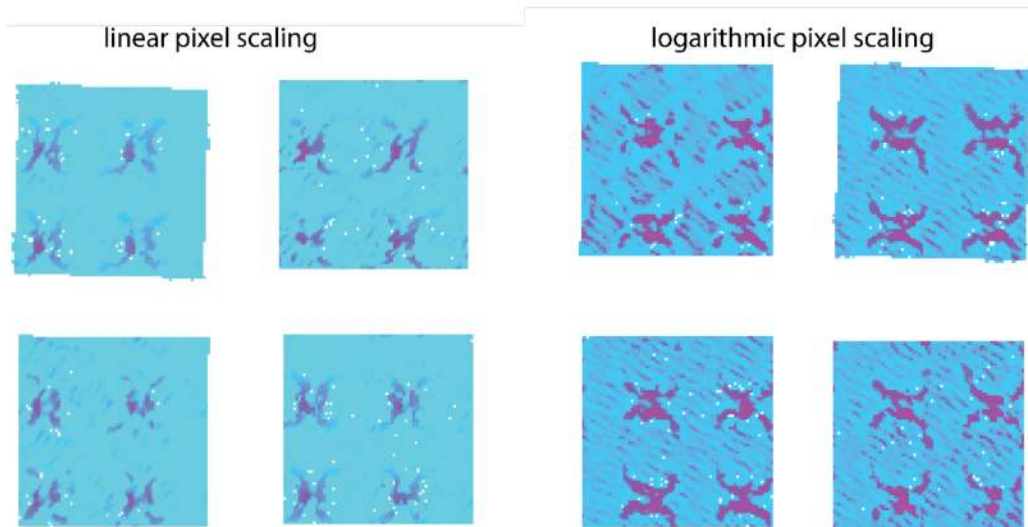


Figure S17. The elastic maps of the kelvin foam cell array.